Sensors and Actuators B 160 (2011) 1565–1572

Contents lists available at SciVerse ScienceDirect

Sensors and Actuators B: Chemical

journal homepage: www.elsevier.com/locate/snb

Quantification of surface acoustic wave induced chaotic mixing-flows in microfluidic wells

Richie J. Shilton, Leslie Y. Yeo, James R. Friend*

MicroNanophysics Research Laboratory, Department of Mechanical Engineering, Monash University and the Melbourne Centre for Nanofabrication, Clayton, Victoria 3800, Australia

ARTICLE INFO

Article history:
Received 2 May 2011
Received in revised form 18 July 2011
Accepted 3 September 2011
Available online 18 September 2011

Keywords:
Microfluidics
Surface acoustic wave
MEMS
Fluid dynamics
Mixing
Chaos

ABSTRACT

We report the use of 20 MHz surface acoustic waves (SAWs) on lithium niobate ($LiNbO_3$) chips to generate fast mixing flows in microfluidic wells. Whilst the chaotic nature of these SAW-driven flows have been speculated in the past, we provide quantitative evidence of the existence of such chaotic advection in these systems over a range of viscosities and input powers through the estimation of the finite time Lyapunov exponent (FTLE), which is a measure of the strength of the chaotic flow. The strongest mixing flows were most evident at higher SAW excitation amplitudes, as expected, since the increasing amounts of inertia in the system served to amplify disturbances in the system that promote the random stretching and folding of the fluid elements over a cascade of length scales in a way that introduces criss-crossing of the streamlines. What is less expected, however, is the effect of fluid viscosity. In contrast to classical acoustic streaming theories where the increase in viscous dissipation is offset by the intensification of the streaming due to increased acoustic energy absorption in systems with larger viscosities, we observe that increases in viscosity essentially suppresses the chaotic advection and hence the mixing effect, which is more akin to most other flow systems. This can be attributed to nonlinear effects due to convective acceleration that cannot be neglected in the *fast streaming* flows induced at the high MHz frequencies associated with the SAWs. The evidence of the chaotic advection in these SAW-driven flows is further verified through a pixel intensity analysis, in which mixing times, quantified through a normalised mixing index, were observed to be inversely proportional to the Lyapunov exponent, characteristic of processes in which transport is dominated by chaotic advection. Practically, these results, which show mixing events taking place in just seconds, demonstrate the utility of SAWs for the design of effective microfluidic mixers.

1. Introduction

There are significant challenges associated with the scaling down of laboratory benchtop fluid flow processes to microscale dimensions, owing to the increasing dominance of capillary and viscous forces over gravitational and inertial forces as the characteristic system dimension is reduced [1,2]. In particular, mixing at small length scales is notoriously difficult given that the multiscale vortical structures that promote effective mixing in turbulent flows are usually absent in microscale flows where the associated hydrodynamic Reynolds number is typically small ($\mathrm{Re} \equiv \rho_f \mathcal{U}\mathcal{L}/\mu \lesssim 1$ wherein ρ_f and μ are the density and dynamic viscosity of the fluid, and $\mathcal{U}$ and $\mathcal{L}$ are the mean velocity and characteristic length scale of the system) and the flow is essentially laminar. Mixing times, characterised by the diffusion time scale $\mathcal{L}^2/\mathcal{D}$ in which $\mathcal{D}$ is the diffusion coefficient, can be prohibitively long, occurring over minutes or even hours, given $\mathcal{D}$ ranges from approximately 10^{-9} m^2/s for small molecules to 10^{-11} m^2/s for complex biological macromolecules. This is often unsatisfactory as mixing in a fast and efficient manner is essential for many applications, including biochemical analysis [3], synthesis and sequencing of nucleic acids [4] and biological processes that involve cell activation [5], enzymatic reaction [6] and protein folding [7].

For microfluidic devices to become commonplace amongst laboratory equipment used by biologists and chemists alike, these limitations associated with mixing at the micro-scale therefore need to be addressed. Whilst conceptually simple, inducing mixing in microfluidic flows by way of passive mixing strategies that integrate topological features such as embedded grooves or baffles, or introducing other flow manipulation designs such as curvature (see, for example, [8,9]), nevertheless involves intricate and expensive fabrication procedures [10]. Active mixing strategies, on the other hand, can circumvent these design inconveniences by exploiting a variety of different energy sources to drive advective transport. Some such active mixers are driven by heating [11], electrokinetics [12], magnetic fields [13], acoustic radiation

* Corresponding author.
E-mail address: james.friend@monash.edu (J.R. Friend).

0925-4005/$ – see front matter © 2011 Elsevier B.V. All rights reserved.
doi:10.1016/j.snb.2011.09.007

[14–16], amongst other external forces [10], though the challenge of incorporating the active component whilst maintaining miniaturisability of the device should not be underestimated.

Whichever the choice of mixing strategy, introducing advective transport into the system in itself is insufficient to enhance mixing. In fact, the Péclet number $\mathrm{Pe} \equiv \mathcal{UL}/\mathcal{D}$, which describes the relative contributions between advection and molecular diffusion in a system, is typically large in microfluidic systems ($\mathrm{Pe} \approx 10$–10^5), suggesting that advection already occurs over a much faster time scale compared to diffusion, and thus any further increases in advective transport simply serves to increase the mixing length, which is proportional to Pe, as long as the Re remains low such that turbulence is absent. The key to promoting effective mixing is to instead introduce *chaotic* advection to disrupt the laminarity of the flow [18–20]. The stretching and folding of the fluid elements associated with such chaotic advection, which correlate to the intersection of fluid streamlines at different and random times, essentially increases the interfacial area and reduces the diffusion length scale (and hence increase the concentration gradient) between the initially segregated species. Owing to the exponential growth of the separation of fluid trajectories in chaotic flows, usually induced by the introduction of periodic modulation of the flow, mixing length scales can be quickly reduced. This therefore allows diffusion to homogenize fluids over increased scalar gradients [21].

There are many difficulties in determining if a fluid system is chaotic. Kim and Beskok described some proposed methods in [22]. Whilst box counting methods can describe the efficiency of mixing, it cannot determine if a system is chaotic. Poincaré sections are useful for visualizing chaotic flows, but cannot aid in determining chaotic strength. On the other hand, *finite time Lyapunov exponents* (FTLE) can quantify both the existence and strength of chaos in flow. FTLE will therefore be used to show that the surface acoustic wave (SAW) driven mixing is chaotic, and to quantify the chaotic strength of these flows and consequent mixing enhancement. The FTLE will then be compared with pixel intensity analysis – a standard mixing efficiency analysis tool.

SAWs are essentially acoustic waves that travel along the surface of an elastic medium, with typical wavelengths in the 10–100 μm range and typical amplitudes on the order of nanometers. Typical SAW devices consist of a pair of interdigital transducers (IDTs) patterned onto a piezoelectric substrate. Common SAW substrates are made of lithium niobate (LN), which allow the propagation of Rayleigh-type waves when the IDT is patterned so that the strain field propagates along the *X*-direction of a 127.68° about-*Y*-cut LN substrate (128YX LN). These waves have energy densities confined to within a few wavelengths of the substrate, and, owing to the transverse-axial nature of the wave, are known to provide good fluid–substrate coupling and thus are an efficient mechanism for driving microfluidic processes. When a SAW is launched from an IDT, its energy is radiated into a fluid drop placed in its path atop the substrate at an angle known as the Rayleigh angle, Θ_R, from an axis normal to the wave propagation (Fig. 1). This radiation arises from the mismatch of sound velocities in the substrate and fluid, and for an infinite half-space, the angle is given by the ratio of the SAW velocity along the substrate along the *X*-direction, c_s, and the sound velocity in the fluid, c_f [14], i.e., $\Theta_R = \sin^{-1}(c_f/c_s)$. At room temperature, $c_s \approx 3990$ m/s in the absence of fluid loading and $c_f \approx 1450$ m/s for water, giving a typical value of $\Theta_R \approx 23°$. Whilst this gives a good approximation of c_s for our case, the correct value of c_s is given by the velocity of the fluid-loaded substrate.

This leakage of radiation in the fluid leads to the generation of a pressure wave in the fluid at the Rayleigh angle, which then drives the acoustic streaming in the fluid [23]. Such streaming flows have been shown in recent years to be potentially effective for many microfluidic applications, depending on the setup and power input; a comprehensive review can be found in [24,25] and the references

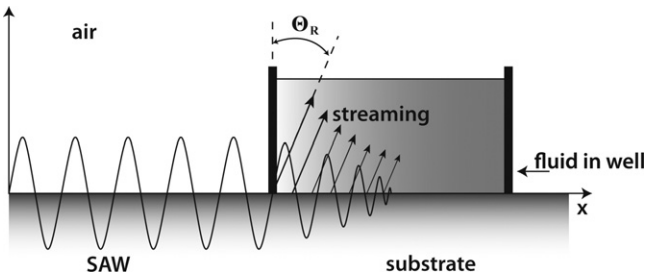

Fig. 1. Schematic illustration showing the energy of the surface acoustic wave radiating into a fluid well at the Rayleigh angle Θ_R and driving bulk recirculation (acoustic streaming) in the fluid (not to scale).

within. In brief, SAWs have been shown to drive flows in channels [26,27] and to drive translation of discrete droplets [28–30,32]. Other fluid manipulation include vibration [33], jetting [34] and atomization [35–37] of droplets. SAWs have also been used to drive particle concentration in droplet microcentrifuges [15,38–40], and using a similar mechanism, have been shown to actively mix fluids [14–16,30,31,40,41]. Whilst [42] suggest that their SAW-driven droplet mixing is chaotic, no quantitative evidence of such chaotic advection is provided. Their method required two tapered IDTs (TIDTs), generating SAW in both the *x* and *y* directions. Further, no mixing of solutions was performed nor was a parametric study conducted on how the fluid properties affect the mixing behaviour. Luong et al. [16] recently characterised acoustically driven mixing with respect to high-throughput flow rates through polydimethylsiloxane (PDMS) channels using varied IDT design, however again, this study did not look into the whether the system was chaotic or not, nor did it study the effects of the fluid properties on the mixing ability of the system. Here, using the FTLE method, we provide, for the first time, quantitative evidence of chaotic advection in a microfluidic well to show how this relates to the efficiency in the mixing process for variations in the fluid viscosity and input power, with the aim of providing further insight to guide the design of SAW-based active microfluidic mixing technology.

2. Materials and methods

The SAW devices in the experiments comprised 0.5 mm thick 128YX LN crystal substrate wafers. Chromium was first deposited via sputtering to provide an adhesion layer of approximately 5 nm. Subsequently, aluminium was deposited to provide a 750 nm layer of aluminium. Each of the straight fingered transducers was then fabricated using standard positive-tone photolithography processes. The transducers were patterned with 8 mm apertures. Our 128YX LN devices run with a coupling coefficient of about $k_{eff} \sim 0.11$. For the operating frequency of 20 MHz, the substrate can no longer be considered a real 'half space', however Laser Doppler Velocimetry (LDV) scans confirmed Rayleigh waves for these devices. There is some loss of acoustic energy to the mounting, determined to be ~10% of acoustic wave energy. This effect, along with any triple-transit or end reflection effects are consistent across the entire dataset, enabling the use of power to compare variables such as the FTLE and mixing indices. Prior to use, the devices were coated with a thin layer of hydrophobic amorphous teflon (Teflon AF, DuPont Corporation), except below where the microfluidic well is placed, so as to prevent the fluid from spreading out from underneath the well during operation. The fluid in the well comprised a mixture of glycerol and water at varying ratios to alter the viscosity of the fluid. Fluorescent, 5 μm polystyrene particle suspensions (BioScientific, Gymea NSM) were introduced in the fluid to aid the flow visualization. The flow was recorded at 20–40 fps using a video camera (Olympus iSpeed, Tokyo, Japan) attached to a

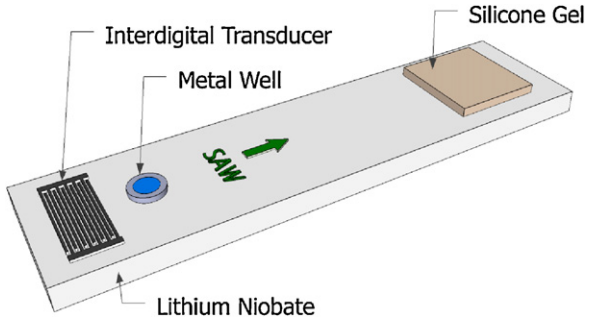

Fig. 2. Schematic depiction of the 20 MHz SAW device in which a microfluidic well is placed within the propagation pathway of the SAW irradiation (not to scale).

stereomicroscope (Olympus BXFM, Tokyo, Japan) using a 5× lens, under fluorescent illumination supplied by an EXFO X-Cite 120 Mercury light source and a 120 W short arc lamp (Olympus, Tokyo, Japan). A steel well, comprised of a 2 mm internal diameter ring, itself extracted from a micro-bearing, was used to house the fluid (Fig. 2). The volume of fluid in the well was kept constant at 2.5 μl in each experiment. The focal plane of the camera was near the surface where the flow was developed. Silicone gel was used to absorb the SAW at the end of the device thus preventing its reflection back towards the well.

An important concern in microfluidics is unwanted heating and evaporation of fluids. All experiments were performed on an aluminium block which acted as a heat sink for any possible excess heating of the device, and were investigated over a short time-span so as to mitigate any heating effects and therefore evaporation of the fluid. Heat sinks, and if necessary Peltier coolers, have been used to avoid heating of SAW devices whilst working with microfluids over longer time periods [17]. This was important especially as the power into the device increased. It was noted that there was negligible evaporation during each run, and the fluid was replaced in between each run to minimise cumulative heating and evaporative volume changes over longer time periods. Owing to the fast mixing times of this method, the device was only required to run on the order of seconds for the higher power (>1 W) experiments, reducing the influence of heating effects.

There are limits to the amplitude of the SAW, as with all ultrasonic piezoelectric devices. The amplitude limit scales inversely with frequency, but the vibration velocity is invariant with respect to frequency at around 1 m/s. Depending on the specific experimental setup, there are also limits associated with power into the fluid, where higher power can lead to translation, jetting, and atomization of fluids in the wavepath [24,25]. There are also time limits associated with heating of the devices if there is no cooling in place. None of these limits were reached in our experiments.

Particle trajectories were tracked using commercially available software, DiaTrack 3.03 (Semasopht, North Epping, Australia), and the particles were assumed to closely follow the flow within the well. The Stokes number, St, representing the ratio of the stopping distance of a particle to a characteristic dimension of an obstacle is defined as

$$\mathrm{St} = \frac{2}{9}\frac{\rho_p}{\rho_f}\left(\frac{a}{\mathcal{L}}\right)^2 \mathrm{Re}, \tag{1}$$

where ρ_p and ρ_f are the particle and fluid densities, respectively, a is the particle radius, $\mathcal{L}$ is the characteristic flow length scale [43]. In all of the experiments to follow, the hydrodynamic $\mathrm{Re} \ll 1$. For the 5 μm particles used, $\mathrm{St} \leq 10^{-6} \ll 1$ and hence it is reasonable to assume that the particle trajectories approximate the flow streamlines, and therefore the particle trajectories can be used to effectively measure the fluid stretch and hence the corresponding FTLE.

Once the flow trajectories of each particle was determined, the coordinate-time vectors of each trajectory were exported into data files for further processing. The flow was parameterized by independently varying the viscosity and input power and recording the particle flows each time. Examples of a frame showing the fluorescent particles in the microfluidic well, in addition to the particle trajectories tracking the flow within the well, can be seen in Fig. 3. After the flow trajectories are reconstructed the trajectories can then be exported in a data file that includes all the spatial and temporal information of each trajectory required to calculate the FTLE estimation according to the method described in the following section.

2.1. Finite time Lyapunov exponent estimation method

Lyapunov exponents are used to quantitatively determine the onset of chaos in a system by measuring the average exponential rate of divergence of the trajectories in a flow [44]. There are a number of Lyapunov exponents that one may define for a flow system; however, when a system's maximal (or largest) Lyapunov exponent is positive, it signifies that there exists exponential growth in the separation of trajectories and hence the system is characteristically chaotic [44]. Specifically, the magnitude of a positive exponent quantifies the relative chaotic strength of the system and can be used to compare different flow systems' mixing abilities, given the strong correlation between the chaotic flow and effective mixing [18]. Any two trajectories driven by the flow with a separation at time $t = 0$ of $|dx(0)|$, may be defined with a relative motion of

$$|dx(t)| \approx e^{\lambda t}|dx(0)|, \tag{2}$$

where λ is the Lyapunov exponent and $\left|dx(t)\right|$ is the separation at time t. For the calculation of the maximal Lyapunov exponent for discrete data, Eq. (2) can be discretised into the FTLE [44,22], given by

$$\lambda = \frac{1}{N\Delta t}\sum_{n=1}^{N} \ln\left(\frac{|dx((n+1)\Delta t)|}{|dx(n\Delta t)|}\right), \tag{3}$$

where λ is now the finite time Lyapunov exponent, n is the iteration variable, Δt is the time interval between iterations, N is the total number of iterations, and $dx(n\Delta t)$ and $dx((n+1)\Delta t)$ are the trajectory separations at time $n\Delta t$ and $(n+1)\Delta t$, respectively [45,22]. This form of the Lyapunov exponent has been implemented in various algorithms used to find the maximal Lyapunov exponent from experimental data. Rosenstein et al. [46] notes that randomly chosen initial conditions will exponentially *separate at a rate dictated by the maximal Lyapunov exponent*.

To determine if the flow in each experiment set was chaotic, and, correspondingly, the magnitude of the chaotic strength, we employed a method that relied on an averaging of the logarithm of the stretch between trajectories over all particles such that the spatial average of the FTLE over the whole two-dimensional plane can be obtained. Owing to the three-dimensional nature of the flow but the two-dimensional visualization method, reconstructed trajectories were created and terminated as the particles moved in and out of the experimental plane of view. For a typical case, the mean number of trajectories in the field of view over the time of the experiment was 970 with a standard deviation of 16. Although a simplification of the FTLE owing to the reduced dimensionality, the present method does account for the *births* and *deaths* of trajectories, as it will continue to average the stretch field across all trajectories and therefore is not reliant on one specific fiducial trajectory. Moreover, the possible out-of-plane velocities occuring in the focal plane, but not accounted for in the two-dimensional reconstruction, may lead to an *under*-estimation rather than an

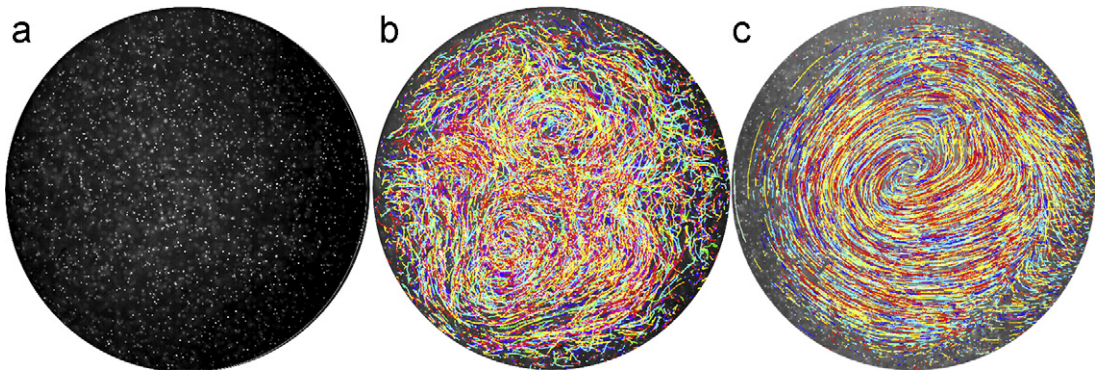

Fig. 3. (a) The white dots show fluorescent particles suspended in the fluid well, captured using a video camera when the fluid is stationary in the absence of any input power: Brownian motion is insignificant. (b) Particle trajectories arising from fluid motion driven by the SAW. The particles are tracked using DiaTrack. Each particle track is represented by a different color. (c) Particle trajectories arising from fluid motion in a high viscosity fluid is far more coherent than for (b) low viscosity fluids under similar excitation conditions, indicated by the more "organized" circumferential particle tracks. (For interpretation of the references to color in this figure legend, the reader is referred to the web version of the article.)

over-estimation of the FTLE in the flow. Out-of-plane trajectories and velocities were minimised in our experiments by excluding a wide range of blurred particles from the particle tracking software. As such, the two-dimensional analysis carried out here is not unreasonable for the purpose of mixing characterisation, and is commonly used throughout the literature even for more complex three-dimensional flows [15,47–51].

We now describe the method used to calculate the FTLE approximation. First, we compared all trajectories with all other trajectories over the entire time of their existence in the plane of view, and found each trajectories' closest neighbour at each time step. We then found the stretch of each closest pair at the next time step and used Eq. (3) to find the FTLE for each trajectory, treating each one as the fiducial trajectory in turn. To account for the folding of the stretched fluid elements, close trajectories were replaced with other, closer trajectories when available at each time step. Lastly, we found a weighted average of these FTLE approximations for all particle trajectories, and this temporal and spatial average was plotted over time. Mathematica 7.0 (Wolfram Research, Champaign, IL, USA) was used to compute the results from the data using this algorithm. In this way we were able to find an approximation to the exponential divergence of the flow field using all available trajectories. This method is nevertheless an approximation owing to the two-dimensional visualization that is a commonly used in the literature as a simplification of three dimensional mixing flows [15,47–51]. It does however allow quantification of the divergence of the flow sufficient to determine if the flow is chaotic in the plane considered, via a positive FTLE approximation, and also allows for comparison between parameter sets in order to determine the optimal conditions for enhanced mixing. We now describe a method to quantify the mixing efficiency in the section to follow.

2.2. Mixing index

The mixing index as a function of time to describe the mixing of a glycerol–water solution with a colored food dye under SAW excitation can be determined from a pixel intensity analysis. For these mixing experiments, a similar setup was used to that in the particle tracking experiments, that is, the same SAW devices were used to drive the mixing, and the same fluids and microfluidic wells were employed. In contrast, however, bright-field illumination was used in place of dark-field fluorescence, and the fluids were illuminated from beneath the clear substrate as the roughly polished counterface of the substrate acted as a light diffuser that aided to suppress specular reflections off the surface associated with the front face of the substrate as well as the free surface of the fluid. Such reflections can erroneously appear to the analysis as fixed, very large particles, and so their suppression is crucial. The extent of mixing was quantified by observing a series of greyscale images over time, extracted from still frames of the video recording, via the following mixing index parameter [13,38,15,52]:

$$C' = \sqrt{\left(\frac{1}{N}\right)\sum_{i=1}^{N}\left(\frac{P_i - \overline{P}}{\overline{P}}\right)^2}, \quad \text{for} \quad 0 \le P_i \le 255, \tag{4}$$

where N is the total number of pixels, P_i is the greyscale intensity of pixel i, and $\overline{P}$ is the mean pixel value $\overline{P} = (1/N)\sum_{i=1}^{N} P_i$. The value of C' should be initially large and tend monotonically towards a small value as the mixing progresses. A normalised mixing index (NMI) that varies between one (unmixed) and zero (mixed) can then be defined:

$$M = \frac{C' - C'_{final}}{C'_{initial} - C'_{final}}, \tag{5}$$

where C'_{final} is C' at the final, fully mixed state, and $C'_{initial}$ is C' at time $t = 0$, prior to the onset of mixing [52].

The mixing index, M, can thus be used to compare the mixing efficiencies across different experimental cases. Here, in particular, they allow for the quantification of the effectiveness of mixing via SAW-driven convection. Mixing indexes generally do not provide information about the dominant mechanism by which mixing occurs, or whether the system is chaotic. We therefore attempt to address this by a comparison between the results obtained from both the FTLE and mixing index analyses. Specifically, the input powers were varied, and dyed fluid (of the same composition/viscosity) was introduced into the well to determine the mixing indices. For comparison, the half-lives of the mixing index, $M_{1/2}$, were calculated to obtain a comparative mixing time across the various experiments. The mixing efficiencies, determined through the pixel intensity analysis across the entire parameter space, can then be compared to the level of chaos, as defined by the FTLE.

3. Results and discussion

Fig. 4 shows the evolution of the FTLE, λ, calculated from Eq. (3), over time for a glycerol–water mixture of viscosity 35.5 mPa s for a range of input powers. In the absence of the SAW-driven convection, the fluid is stationary and mass transport occurs by diffusion alone, as seen by the zero value of λ for all times. When the SAW is applied as an external energy source, it can be seen that non-zero

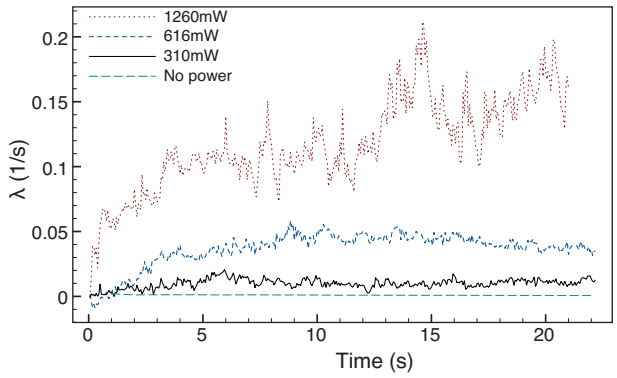

Fig. 4. Maximal Lyapunov exponent λ over time, as a function of the input power for a glycerol–water fluid mixture with viscosity 35.5 mPa s.

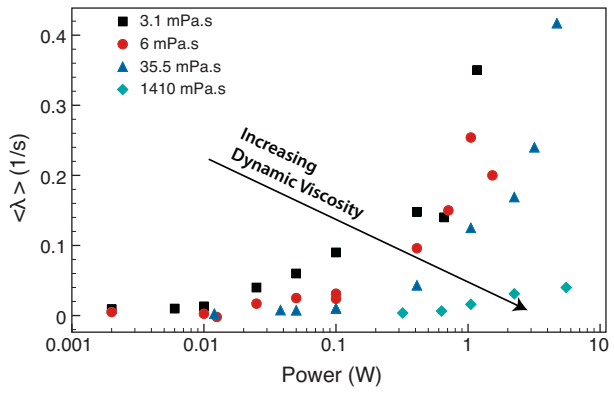

Fig. 6. Mean values of the FTLE ⟨λ⟩ for different fluid viscosities over a range of input powers.

values for λ are obtained, which initially increases over an initial transient but approaches a steady-state value. A more meaningful way to compare values of λ is to calculate its mean value ⟨λ⟩ over a sufficiently large period after the initial transient region. This is shown in Fig. 5 for varying average particle velocities ⟨*V*⟩.

We observe the mean values for λ to increase with increasing input power. This is because of an increasing amount of SAW energy into the fluid resulting in an intensification of the acoustic streaming (bulk liquid recirculation) in the fluid, as observed by the increasing average fluid velocities measured within the fluid (Fig. 5). This increase in the fluid inertia amplifies disturbances present in the system and leads to an increasing amount of chaotic advection in the fluid volume, as seen by the vortices that arise over a cascade of length scales and the symmetry-breaking cross-flow streamlines (Fig. 3(b)). Consequently, we expect the mixing length and hence the mixing time to decrease, as will be confirmed subsequently through the comparison with the mixing experiments and quantified through the pixel intensity analysis. It is also interesting to note that when even a very small amount of power is applied to the device, positive values of ⟨λ⟩ are obtained, though small in magnitude (Fig. 6). This shows that when there is even a small amount of acoustic streaming in the fluid well, there is on average a positive value of the exponential divergence of the flow field, that is, the flow is seen to be weakly chaotic even at low powers.

The effect of varying the fluid viscosity on the mean values of the FTLE can be seen in Fig. 6 from which we observe that, at any set power, ⟨λ⟩ increases for fluids of decreasing viscosity, owing to the decrease in the associated viscous damping, itself responsible for suppressing disturbances in the system. This suppresses the chaotic flow field that gives rise to the crossing of streamlines necessary to drive efficient mixing. For fluids possessing lower viscosities, an increase in input power is seen to drive larger inertial streaming velocities, thus resulting in stronger chaotic advection within the system and hence increases in the FTLE. This is consistent with the data plotted in Fig. 7 that shows the relationship between ⟨λ⟩ and the average particle velocity; note the exponential increase in ⟨λ⟩ as the average velocity increases. On the other hand, the flow is increasingly damped as the viscosity is increased due to viscous drag that suppresses the chaotic flow and hence the mixing. At high viscosities, the chaotic flow reverts to almost bulk rotational flow, as seen in Fig. 3(c) in which the fluid elements only weakly diverge: their separation remains fairly constant as they travel along the concentric streamlines associated with simple rotational flow. Nevertheless, we note that even in the high viscosity systems considered here chaos remains with positive, albeit small ⟨λ⟩ values, indicating less chaotic flow than in the low viscosity systems.

Whilst such behaviour is expected in most fluid flows, these observations are not entirely expected in acoustically driven flows. Particularly, and quite importantly, they differ from that observed by Lighthill [53], and those that preceded him [54–57], who noted that the strength of the acoustic streaming is unaffected by changes in viscosity. This is because the increased absorption of the acoustic wave and hence the concomitant increase in the acoustic streaming intensity in fluids of larger viscosity is exactly offset by the

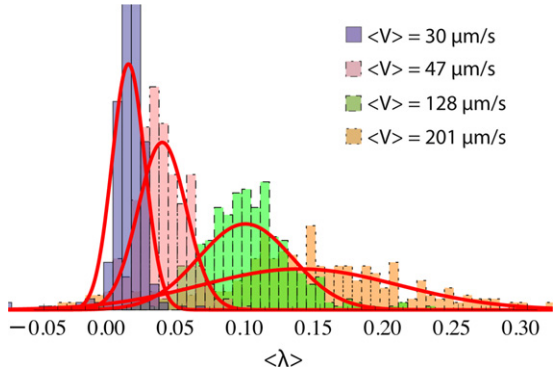

Fig. 5. The bar plots show the distribution of the FTLE over time as the dye is homogenized for a fixed input power, as shown in Fig. 4, whereas the red curves are normal fits to the Lyapunov exponent data. Both the mean value and standard deviation are observed to increase with increasing input power. The average fluid velocity measured is also observed to increase with input power. (For interpretation of the references to color in this figure legend, the reader is referred to the web version of the article.)

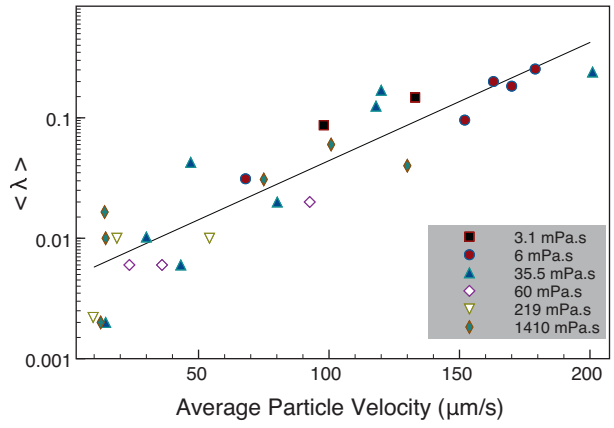

Fig. 7. Relationship between the measured average particle (and hence fluid) velocity and the mean value of the FTLE ⟨λ⟩ for a range of fluid viscosities. The least squares fit of the data is shown with $R^2 = 0.84$.

increased viscous drag that acts to retard the flow. Lighthill's observation that acoustic streaming is independent of the fluid viscosity, however, is predicated on *slow streaming* – the case in which the *streaming* Reynolds number ($\mathrm{Re}_s \equiv \rho_f \mathcal{U}_1 \mathcal{L}/\mu \ll 1$, where $\mathcal{U}_1$ is now the characteristic flow velocity incorporating both the fluid velocity and the effect of the acoustic wave propagation) [58–60,25] is small: the second order acoustic streaming velocities from the successive approximation is significantly smaller than the first-order fluid element velocities driven by the acoustic wave itself. In our experiments, however, Re_s is typically greater than 1 – the case of *fast streaming* – thus rendering this assumption invalid. We use Riley's equation to calculate our acoustic streaming velocity from $\mathcal{U}_1 = 2(PS_b/\rho_f c\mathcal{L}^4)^{1/2}$, where P is the power measured in Watts emitted by the acoustic source and c is the sound speed [59]. If all of the input power was converted to acoustic energy in the droplet, for the low viscosity case we would find that the $\mathrm{Re}_s \sim 100\text{–}5000 \gg 1$. In reality, significant power loss occurs at the device input, and at the solid–fluid interface. However, even taking this loss into account, we find Re_s is still several orders of magnitude above 1. This power loss can be estimated by determining the reflected power at the device input, as well as the rate of power transmission from the mechanical surface wave into the droplet, which is estimated at ~33%. Interestingly, for the high viscosity case we find Re_s ranges from ~0.2 to 5, approaching the region where the flow only encounters resistance from viscosity and exhibits linear behaviour [25]. This helps to explain the suppressed chaotic nature of the high viscosity flows that approach the slow streaming region. For fluid flow with associated acoustic wave propagation, the streaming Reynolds number is more meaningful than the hydrodynamic Reynolds number. That the increase in acoustic streaming due to viscous absorption is not exactly offset by the decrease in fluid flow due to viscous dissipation may be attributed to nonlinear effects, particularly the convective acceleration and the compressibility [61,25], the latter appearing through the quadratic term in the equation of state [62] – such nonlinear effects cannot typically be neglected for acoustic streaming at the high (MHz order) frequencies employed here, and are a problem in classical analyses where continued fractions and perturbation theory based on an expansion using the Mach number are used [25].

Fig. 8 shows that in the presence of the SAW-induced chaotic advection, the dye is observed to quickly homogenize throughout the fluid well. Similar images were obtained for different input powers. The mixing process is formally quantified in Fig. 9, where the NMI values were calculated using Eqs. (4) and (5), therefore showing the rate at which the dye is homogenized for a range of input powers (NMI has a value of 1 when the fluid is initially unmixed and approaches 0 as the dye becomes completely mixed as $t \to \infty$). Periodic fluctuation, which are present and can be attributed to the temporal variations in how the dye elements stretch and fold. The frequency of these fluctuations increases as the input power, and therefore the fluid velocity is increased. The results in Figs. 8 and 9 confirm the fluid is well mixed throughout the whole fluid, with no islands of inhomogeneity (poorly mixed local regions in the fluid in which mass transport with the rest of the fluid body only occurs via molecular diffusion) that pose an obstacle to efficient mixing. This verifies (qualitatively) the FTLE calculation and provides confidence in our use of a global spatial average of the FTLE and the two-dimensional approximation.

Particles were tracked under the same conditions as the dye experiments shown in Fig. 9, and the mean Lyapunov exponent computed from the identified particle trajectories for comparison with the results from the pixel intensity analysis. More specifically, the half-lives of the mixing indices $M_{1/2}$ were used as an arbitrary measure for comparing the mixing rates against the Lyapunov times at different input powers; a linear fit was used over the

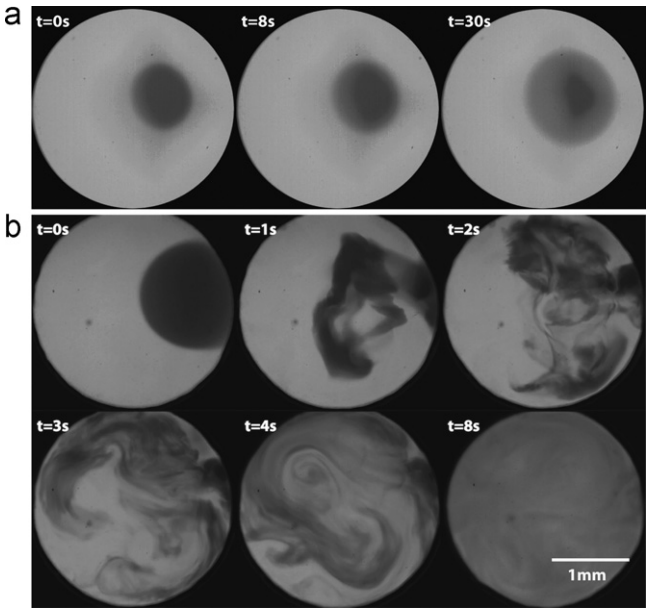

Fig. 8. Images showing (a) mixing of a coloured dye due to pure diffusion when the fluid is not excited by the SAW, and (b) mixing under chaotic flow conditions driven by the SAW with an input power of ~1 W. The fluid viscosity is 35.5 mPa s. These images were extracted from the video recordings acquired at 20 fps.

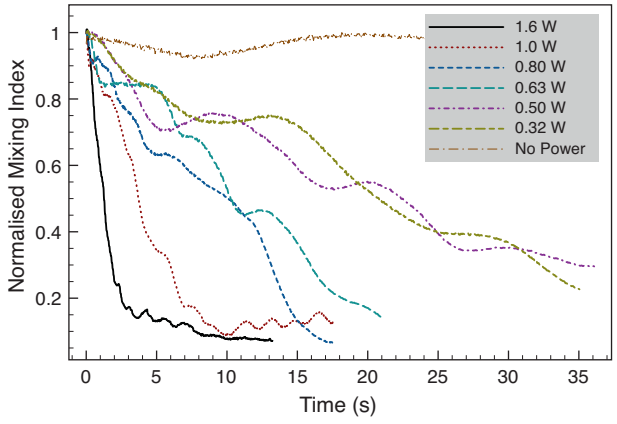

Fig. 9. Normalised mixing index as a function of time for different input powers. The mixing time is seen to reduce with increasing input power. We note that purely diffusive mixing occurs over time scales significantly longer than that shown, as seen in the case with no applied power. (For interpretation of the references to color in artwork, the reader is referred to the web version of the article.)

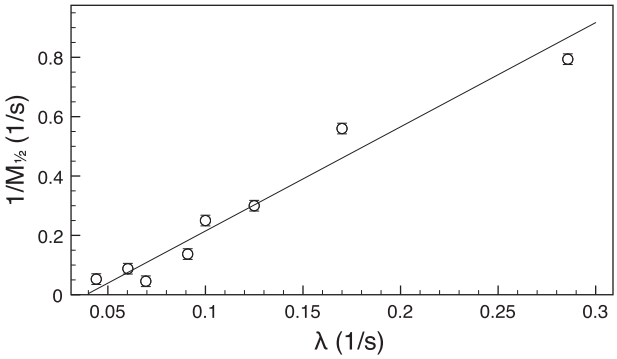

Fig. 10. Comparison of the inverse mixing half-lives, $1/M_{1/2}$, against the Lyapunov exponent approximation, λ. The Lyapunov exponents are seen to scale linearly with the inverse mixing half-lives, as is expected for mixing dominated by chaotic flow.

initial NPI region to smooth out the fluctuations in the NPI values seen in Fig. 9. Fig. 10 shows that the inverse mixing half-lives scale linearly with the mean Lyapunov times, characteristic of chaotic-dominated transport [45], therefore providing yet further evidence of chaotic advection in the SAW-driven mixing and supporting the idea of a two dimensional model as useful to the prediction of fully three dimensional mixing.

4. Conclusions

In this work, SAW-driven chaotic flows in microfluidic wells have been investigated and an estimation of the FTLE was used to characterise the chaotic strength of the flow using all available particle trajectories. This maximal FTLE estimation method relies on finding the trajectories of a significant number of particles (~800–1000 at any time) obtained through flow visualization; these trajectories are then used to calculate the FTLE for all particles, from which a mean FTLE $\langle\lambda\rangle$ over a sufficiently large period can be computed. This result provides a quantification of the spatial average of the FTLE, and the exponential divergence of the flow elements, and when positive, provides evidence that a flow system is chaotic. Using this method, SAW-driven chaotic mixing flows in microfluidic wells have been demonstrated and quantified for the first time, and these flows can be exploited to drive enhanced mixing. Generally, the larger the acoustic excitation energy, the larger the fluid inertia in the system to drive chaotic advection. This has implications on the effect of the fluid viscosity on the system. Unlike other fluid flows where the fluid viscosity acts only to dissipate the energy within the system and hence suppress the chaotic advection, the viscosity in acoustically driven flows also aids the absorption of the sound energy to drive the fluid flow. In classical theories where the streaming Reynolds number is small, i.e., for slow streaming, the effect of viscosity is therefore often neglected. On the contrary, we show that viscous absorption and dissipation effects are not exactly balanced due to nonlinear convective and compressibility effects that become important as the streaming Reynolds number grows beyond one. Overall, however, we find the fluid viscosity acts to reduce the chaotic advection, as seen in other fluid flows. In addition, a mixing index was used to quantify the rate at which dye is homogenized within the fluid well. The linear relationship between the inverse mixing time and $\langle\lambda\rangle$ as a characteristic of transport within the fluid, is dominated by chaotic mixing, further confirming the existence of chaotic advection in SAW-driven mixing. In any case, the utility of enhanced mixing due to the SAW-induced chaotic advection, typically completing within seconds, demonstrates its potential for fast micromixing in integrated portable biomicrofluidic chip technologies.

Acknowledgements

This work was supported by Australian Research Council Discovery Grants DP0666660, DP0773221, DP0985253 and DP1092955 and the CSIRO Flagship Project Grant on Novel Sensors for Water Quality.

References

[1] T.M. Squires, S.R. Quake, Microfluidics: fluid physics at the nanoliter scale, Rev. Mod. Phys. 77 (2005) 977–1026.
[2] L.Y. Yeo, H.-C. Chang, P.P.Y. Chan, J.R. Friend, Microfluidic devices for bioapplications, Small 7 (2011) 12–48.
[3] K.A. Shaikh, K.S. Ryu, E.D. Goluch, J.-M. Nam, J. Liu, A modular microfluidic architecture for integrated biochemical analysis, Proc. Natl. Acad. Sci. U.S.A. 102 (2005) 9745–9750.
[4] P.A. Auroux, D. Iossifidis, D.R. Reyes, A. Manz, Micro total analysis systems. 2. Analytical standard operations and applications, Anal. Chem. 74 (2002) 2637–2652.
[5] C. Ionescu-Zanetti, R.M. Shaw, J. Seo, Y.-N. Jan, L.Y. Jan, Mammalian electrophysiology on a microfluidic platform, Proc. Natl. Acad. Sci. U.S.A. 102 (2005) 9112–9117.
[6] C.K. Fredrickson, Z.H. Fan, Macro-to-micro interfaces for microfluidic devices, Lab Chip 4 (2004) 526–533.
[7] D.E. Hertzog, X. Michalet, M. Jäger, X. Kong, J.G. Santiago, S. Weiss, O. Bakajin, Femtomole mixer for microsecond kinetic studies of protein folding, Anal. Chem. 76 (2004) 7169–7178.
[8] A.D. Stroock, S.K.W. Dertinger, A. Ajdari, I. Mezić, H.A. Stone, G. Whitesides, Chaotic mixer for microchannels, Science 295 (2002) 647–651.
[9] A. Sudarsan, V. Ugaz, Multivortex micromixing, Proc. Natl. Acad. Sci. U.S.A. 103 (2006) 7228–7233.
[10] N.-T. Nguyen, Z. Wu, Micromixers – a review, J. Micromech. Microeng. 15 (2005) R1–R16.
[11] J.-H. Tsai, L. Lin, A thermal-bubble-actuated micronozzle-diffuser pump, J. Microelectromech. Syst. 11 (2002) 665–671.
[12] H.-C. Chang, L.Y. Yeo, Electrokinetically Driven Microfluidics and Nanofluidics, Cambridge University, 2010.
[13] L.-H. Lu, K.S. Ryu, C. Liu, A magnetic microstirrer and array for microfluidic mixing, J. Microelectromech. Syst. 11 (2002) 462–469.
[14] A. Wixforth, C. Strobl, C. Gauer, A. Toegl, J. Scriba, Z.V. Guttenberg, Acoustic manipulation of small droplets, Anal. Bioanal. Chem. 379 (2004) 982–991.
[15] R. Shilton, M.K. Tan, L.Y. Yeo, J.R. Friend, Particle concentration and mixing in microdrops driven by focused surface acoustic waves, J. Appl. Phys. 104 (2008) 014910.
[16] T.D. Luong, V.N. Phan, N.T. Nguyen, High-throughput micromixers based on acoustic streaming induced by surface acoustic wave, Microfluid. Nanofluid. 10 (2011) 619–625.
[17] K. Kulkarni, J. Friend, L. Yeo, P. Perlmutter, N.T. Nguyen, High-throughput micromixers based on acoustic streaming induced by surface acoustic wave, Microfluid. Nanofluid. 10 (2011) 619–625.
[18] G.A. Voth, G. Haller, J.P. Gollub, Experimental measurements of stretching fields in fluid mixing, Phys. Rev. Lett. 88 (2002) 254501.
[19] J.M. Ottino, S. Wiggins, Designing optimal micromixers, Science 305 (2004) 485–486.
[20] S. Wiggins, J.M. Ottino, Foundations of chaotic mixing, Philos. R. Soc. A 362 (2004) 937–970.
[21] J.M. Ottino, S. Wiggins, Introduction: mixing in microfluidics, Philos. Trans. R. Soc. A 362 (2004) 923–934.
[22] H.J. Kim, A. Beskok, Quantification of chaotic strength and mixing in a micro fluidic system, J. Micromech. Microeng. 17 (2007) 2197–2210.
[23] L. Rayleigh, On waves propagated along the plane surface of an elastic solid, Proc. Lond. Math. Soc. 1 (1885) 4–11.
[24] L.Y. Yeo, J.R. Friend, Ultrafast microfluidics using surface acoustic waves, Biomicrofluidics 3 (2009) 012002.
[25] J. Friend, L. Yeo, Microscale acoustofluidics: microfluidics driven via acoustics and ultrasonics, Rev. Mod. Phys. 83 (2011) 647.
[26] M. Cecchini, S. Girardo, D. Pisignano, R. Cingolani, F. Beltram, Acoustic-counterflow microfluidics by surface acoustic waves, Appl. Phys. Lett. 92 (2008) 104103.
[27] M.K. Tan, L.Y. Yeo, J.R. Friend, Rapid fluid flow and mixing induced in microchannels using surface acoustic waves, Europhys. Lett. 87 (2009) 47003.
[28] M.K. Tan, J.R. Friend, L.Y. Yeo, Microparticle collection and concentration via a miniature surface acoustic wave device, Lab Chip 7 (2007) 618–625.
[29] X.Y. Du, Y.Q. Fu, J.K. Luo, A.J. Flewitt, W.I. Milne, Microfluidic pumps employing surface acoustic waves generated in ZnO thin films, J. Appl. Phys. 105 (2009) 024508.
[30] Y. Bourquin, J. Reboud, R. Wilson, Tuneable surface acoustic waves for fluid and particle manipulations on disposable chips, Lab Chip 10 (2010) 1898–1901.
[31] A.-L. Zhang, Z-Q. Wu, X.-H. Xia, Transportation and mixing of droplets by surface acoustic wave, Talanta 84 (2011) 293–297.
[32] P. Brunet, M. Baudoin, O.B. Matar, F. Zoueshtiagh, Droplet displacements and oscillations induced by ultrasonic surface acoustic waves: a quantitative study, Phys. Rev. E 81 (2010) 036315.
[33] H. Li, J.R. Friend, L.Y. Yeo, Microfluidic colloidal island formation and erasure induced by surface acoustic wave radiation, Phys. Rev. Lett. 101 (2008) 084502.
[34] M.K. Tan, J.R. Friend, L.Y. Yeo, Interfacial jetting phenomena induced by focused surface vibrations, Phys. Rev. Lett. 103 (2009) 24501.
[35] M. Kurosawa, T. Watanabe, A. Futami, T. Higuchi, Surface acoustic wave atomizer, Sens. Actuators 50 (1995) 69–74.
[36] A. Qi, L.Y. Yeo, J.R. Friend, Interfacial destabilization and atomization driven by surface acoustic waves, Phys. Fluids 20 (2008) 074103.
[37] S.R. Heron, R. Wilson, S.A. Shaffer, D.R. Goodlett, J.M. Cooper, Surface acoustic wave nebulization of peptides as a microfluidic interface for mass spectrometry, Anal. Chem. 82 (2010) 3985–3989.
[38] H. Li, J.R. Friend, L.Y. Yeo, Surface acoustic wave concentration of particle and bioparticle suspensions, Biomed. Microdev. 9 (2007) 647–656.
[39] R.V. Raghavan, J.R. Friend, L.Y. Yeo, Particle concentration via acoustically driven microcentrifugation: microPIV flow visualization and numerical modelling studies, Microfluid. Nanofluid. 8 (2010) 73–84.

[40] M. Alghane, B. Chen, Y. Fu, Y. Li, J.K. Luo, A.J. Walton, Experimental and numerical investigation of acoustic streaming excited by using a surface acoustic wave device on a 128° YX-$LiNbO_3$ substrate, J. Micromech. Microeng. 21 (2011) 015005.
[41] A. Renaudin, V. Chabot, E. Grondin, V. Aimez, P.G. Charette, Integrated active mixing and biosensing using surface acoustic waves (SAW) and surface plasmon resonance (SPR) on a common substrate, Lab Chip 10 (2010) 111–115.
[42] T. Frommelt, M. Kostur, M.W. Schäfer, P. Talkner, P. Hänggi, A. Wixforth, Microfluidic mixing via acoustically driven chaotic advection, Phys. Rev. Lett. 100 (2008) 034502.
[43] N.T. Ouellette, P.J.J. O'Malley, J.P. Gollub, Transport of finite-sized particles in chaotic flow, Phys. Rev. Lett. 101 (2008) 174504.
[44] A. Wolf, J.B. Swift, H.L. Swinney, J.A. Vastano, Determining Lyapunov exponents from a time series, Physica D 16D (1984) 285–317.
[45] Y.-K. Lee, C. Shih, P. Tabeling, C.-M. Ho, Experimental study and nonlinear dynamic analysis of time-periodic micro chaotic mixers, J. Fluid Mech. 575 (2007) 425–448.
[46] M.T. Rosenstein, J.J. Collins, C.J.D. Luca, A practical method for calculating largest Lyapunov exponents from small data sets, Physica D 65 (1993) 117–134.
[47] V. Hessel, H. Lowe, F. Schonfeld, Micromixers – a review on passive and active mixing principles, Chem. Eng. Sci. 60 (2005) 2479–2501.
[48] T.G. Kang, T.H. Kwon, Colored particle tracking method for mixing analysis of chaotic micromixers, J. Micromech. Microeng. 14 (2004) 891–899.
[49] S. Lee, H. Kang, B. Choi, A study on the novel micromixer with chaotic flows, Microsyst. Technol. (2009) 269–277.
[50] R.H. Liu, M.A. Stremler, K.V. Sharp, M.G. Olsen, J.G. Santiago, R.J. Adrian, H. Aref, D.J. Beebe, Passive mixing in a three-dimensional serpentine microchannel, J. Microelectromech. Syst. 9 (2000) 190–197.
[51] C.L. Sun, J.Y. Sie, Active mixing in diverging microchannels, Microfluid. Nanofluid. 8 (2010) 485–495.
[52] T. Roy, A. Sinha, S. Chakraborty, R. Ganguly, I.K. Puri, Magnetic microsphere-based mixers for microdroplets, Phys. Fluids 21 (2009) 027101.
[53] J. Lighthill, Acoustic streaming, J. Sound Vib. 61 (1978) 391–418.
[54] W.L. Nyborg, Acoustic streaming due to attenuated plane waves, J. Acoust. Soc. Am. 25 (1953) 68–75.
[55] P.J. Westervelt, The theory of steady rotational flow generated by a sound field, J. Acoust. Soc. Am. 26 (1953) 60–67.
[56] J.T. Stuart, Laminar Boundary Layers, Oxford University, 1963.
[57] L. Rayleigh, The Theory of Sound: In Two Volumes, Macmillan, 1986.
[58] V.V. Krylov, Noise and Vibration from High-speed Trains, Thomas Telford, 2001.
[59] N. Riley, Acoustic streaming, Theor. Comp. Fluid Dyn. 10 (1998) 349–356.
[60] N. Riley, Steady streaming, Annu. Rev. Fluid Mech. 33 (2001) 43–65.
[61] L.K. Zarembo, V.A. Krasil'nikov, Some problems in the propagation of ultrasonic waves of finite amplitude in liquids, Sov. Phys. Usp. 2 (1959) 580–599.
[62] R.T. Beyer, Parameter of nonlinearity in fluids, J. Acoust. Soc. Am. 32 (1960) 719–721.

Biographies

Richie Shilton is a current PhD student in the MicroNanophysics Research Laboratory at Monash University, where he is expected to complete his PhD by the end of 2011. Richie completed his joint Bachelor of Engineering (mechanical)/Bachelor of Science (maths/physics) with first class honours at Monash University in 2007. Under the supervision of Prof. James Friend and Assoc. Prof. Leslie Yeo, Richie is investigating surface acoustic wave interactions with microfluids and solids. He is using surface acoustic waves to actuate high speed rotations with applications in chaotic micromixing, centrifugal microfluidics, and fluid coupled micromotors.

Leslie Yeo received his Ph.d. degree from Imperial college london in 2002, for which he was awarded the Dudley Newitt prize for a computational/theoretical thesis of outstanding merit. He is currently an Australian Research Fellow and Associate Professor in the Department of Mechanical Engineering and Co-Director of the Micro/Nanophysics Research Laboratory at Monash University, Australia. Prior to joining Monash University, he was a Mathematical Modeller at Det Norske Veritas UK and a Postdoctoral Research Associate in the Department of Chemical & Biomolecular Engineering at the University of Notre Dame, Indiana. Dr. Yeo was the recipient of the 2007 Young Tall Poppy science award from the Australian Institute for Policy & Science "in recognition of the achievements of outstanding young researchers in the sciences including physical, biomedical, applied sciences, engineering and technology," and both the Dean and Vice-Chancellor's awards for Excellence in Early Career Research. His work on microfluidics has been featured widely in the media, for example, on the Australian Broadcasting Corporation's science television program Catalyst, 3RRR radio broadcast, and in various articles in The Economist, New Scientist, The Washington Times, The Age, and The Sydney Morning Herald, in addition to being highlighted in Nature and Science. Dr. Yeo is co-author of the book Electrokinetically Driven Microfluidics & Nanofluidics (Cambridge University Press), and the author of over 90 research publications and over 15 patent applications. He is also an Editor of the American Institute of Physics journal Biomicrofluidics.

James Friend joined Monash University in late 2004 having been an assistant professor at the Tokyo Institute of Technology's Precision and Intelligence Laboratory from 2001-4. He co-founded and co-directs the £7.5 million MicroNanophysics Research Laboratory with a current staff of 3 academics, 4 post-doctorates and 8 PhD students. A professor in the Department of Mechanical Engineering at Monash University and an MCN Tech Fellow at the Melbourne Centre for Nanofabrication, he has research interests in micro/nanodevices for biomedical applications. He is an associate editor of Biomicrofluidics and is a member of the IEEE Nanotechnology for Biology and a pair of Ultrasonics Technical Committees, and has over 120 peer-reviewed publications and twenty-five patents and patent applications. He received excellence in teaching, early career research, and research awards from the Monash Faculty of Engineering in 2006, 2008, and 2011, respectively, a Future Leader award from the Davos Future Summit in 2008, and was awarded as a Top 10 emerging scientific leader of Australia by Microsoft and The Australian newspaper in 2009.